

Stability of Organic Cations in Solution-Processed $\text{CH}_3\text{NH}_3\text{PbI}_3$ Perovskites: Formation of Modified Surface Layers

A. Calloni,^{*,†} A. Abate,[‡] G. Bussetti,[†] G. Berti,[†] R. Yivlialin,[†] F. Ciccacci,[†] and L. Duò[†]

[†]Dipartimento di Fisica, Politecnico di Milano, Piazza Leonardo Da Vinci, 32, 20133 Milano, Italy

[‡]Adolphe Merkle Institute, University of Fribourg, Ch. du. Musée 3, CH-1700 Fribourg, Switzerland

Received: June 7, 2015

Revised: August 8, 2015

Published: August 19, 2015

■ INTRODUCTION

Organic perovskites, featuring a direct bandgap, a high absorption coefficient, and excellent charge transport characteristics, have recently emerged as one of the most promising active materials for the next generation of solar cells,¹ with current power conversion efficiencies certified at 20.1%.² The electronic and structural characteristics of this hybrid material, made of a nearly cubic metal halide cage surrounding an organic cation, can be tuned by modifying the chemical composition of the two constituent parts. Compact crystalline films of organic–inorganic perovskite can be produced according to a variety of different methods, ranging from solution processing in a single³ or in multiple steps⁴ to vacuum deposition,⁵ atomic layer deposition,⁶ and vapor-assisted solution processing,⁷ each of them leading, after careful optimization, to efficient photovoltaic devices. At present, the most investigated organic–inorganic perovskites are identified by the formula $\text{CH}_3\text{NH}_3\text{PbX}_3$, with $X = \text{Cl}, \text{Br}, \text{or I}$, and they are synthesized by mixing methylammonium (MA) and lead halide (PbX_2) salts. Particular mixed halide perovskites are prepared from a solution of lead chloride (PbCl_2) and methylammonium iodide (MAI), and they are commonly indicated with the chemical formula $\text{MAPbI}_{3-x}\text{Cl}_x$. The latter formulation enabled preparing perovskite films with superior charge transport characteristics, which have been used to make photovoltaic devices with an efficiency similar to the best established for inorganic technologies.^{3,8} Although the details of the underlying physicochemical processes are still under debate, several studies concluded about the active role of Cl atoms in seeding the crystallization process of the MAPbI_3 phase,⁹ thus

improving the morphology of the perovskite films and therefore reducing the charge scattering.

In the following, we will consider the chemical composition and the electronic structure of solution-processed $\text{MAPbI}_{3-x}\text{Cl}_x$ perovskites. We detect the spectroscopic features of methylamine molecules, a byproduct of the chemical reaction leading to the formation of the perovskite structure from its chemical precursors. Starting from freshly made perovskite films, we follow *in situ* the changes in the electronic structure at the perovskite surface upon vacuum annealing and sputtering, which promote the release of organic species from the surface and the stabilization of a passivating lead iodide (PbI_2) overlayer.^{10,11} The band alignment at the $\text{MAPbI}_3/\text{PbI}_2$ interface clearly indicates the presence of a significant energy barrier influencing the extraction of charges from the perovskite layer.

■ EXPERIMENTAL DETAILS

The perovskite samples were produced by either spin-coating or vacuum evaporation. For the spin-coated samples we followed the procedure explained in refs 3 and 12: a porous Al_2O_3 layer was first deposited by spin-coating 100 μL of alumina suspension on a glass substrate covered with fluorine-doped tin oxide and sintering at 150 °C for 15 min. About 100 μL of methylammonium iodide (MAI) and lead chloride (PbCl_2) in dimethylformamide (3:1 molar ratio) was then spin-coated and annealed for 1 h at 100 °C. For the evaporated

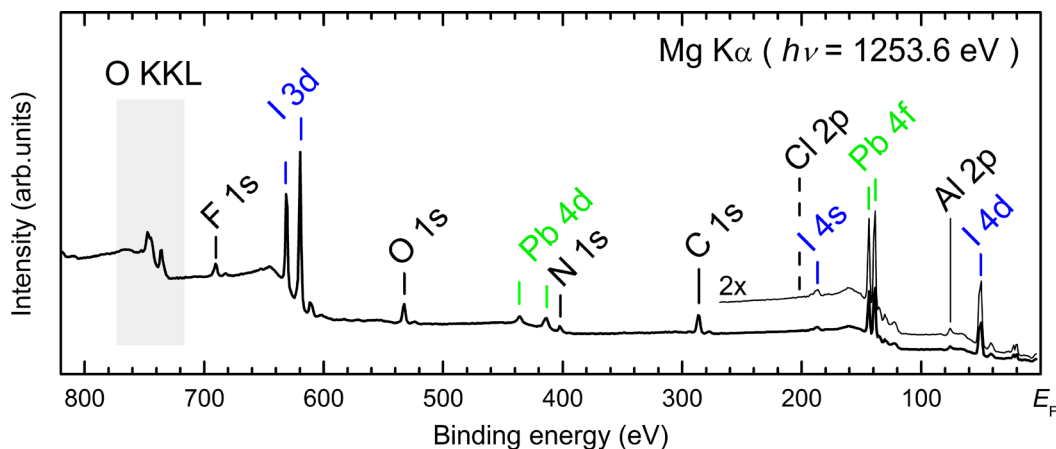


Figure 1. XPS wide scan from a representative as-received $\text{CH}_3\text{NH}_3\text{PbI}_{3-x}\text{Cl}_x$ sample at normal electron emission (pass energy 40 eV).

samples, a conductive p-doped Si substrate was used. The perovskite layer was formed through the coevaporation of PbCl_2 and MAI, as explained in ref 5. The deposited film was then annealed at 100°C for 45 min. Both strategies resulted in the formation of a perovskite layer with a nominal $\text{MAPbI}_{3-x}\text{Cl}_x$ composition, a thickness of about 100 nm, and a black appearance. The samples were fixed to a Ta sample holder by means of a vacuum-compatible epoxy, and the sample surface was electrically connected to the holder by means of Ta stripes. The entire sample preparation procedure, which consisted in growing the perovskite layers (by either spin-coating or vacuum evaporation), annealing the samples, and positioning them on the Ta holders took place inside a N_2 -filled glovebox. The samples were then transported in a nitrogen filled enclosure and swiftly inserted into the vacuum chamber housing the electron spectrometer. The overall exposure time to ambient conditions was less than 1 min.

The photoemission study was performed in an ultrahigh-vacuum (UHV) system (the base pressure was in the low 10^{-8} Pa range) described in detail elsewhere.¹³ The system is equipped with a 150 mm hemispherical analyzer operated at a pass energy of 20 eV (unless otherwise stated) for XPS and 0.5 eV for UPS, yielding an overall full width at half-maximum (fwhm) resolution of about 0.9 and 0.05 eV, respectively. Photoelectrons were excited by $\text{Mg K}\alpha$ radiation ($h\nu = 1253.6$ eV) for XPS. UV radiation was obtained from a He discharge lamp (He I and He II lines at 21.2 and 40.8 eV, respectively). Source satellites were always subtracted. For UPS, both the energy scale and the resolution were calibrated by fitting a complementary error function to the Fermi edge of a polycrystalline Au specimen. We collected electrons emitted an angle of both 0° (normal emission) and 60° (grazing emission) from the surface normal. The work function was measured from the threshold energy for the emission of secondary electrons during He I excitation. In the latter case, a negative potential of -10 V was applied to the sample according to the method of ref 14. All measurements were performed with the samples kept at room temperature; several scans were acquired for each spectrum without any noticeable evolution in the photoemission line shape. Additional treatments performed *in situ* comprised (i) vacuum annealing at increasing temperature, up to 150°C , monitored by means of a thermocouple placed in close contact with the sample holder, and (ii) surface erosion by sputtering. We employed a rastered Ar^+ beam impinging on the sample surface at grazing incidence (60° from the surface

normal). The beam current density and the acceleration potential for the ions were adjusted to $1.5 \mu\text{A}\cdot\text{cm}^{-2}$ and 1.5 keV, respectively.

RESULTS AND DISCUSSION

Chemical Characterization of the As-Received Perovskite.

Figure 1 shows an X-ray photoemission spectroscopy (XPS) wide scan taken from a representative $\text{MAPbI}_{3-x}\text{Cl}_x$ perovskite sample spin-coated on Al_2O_3 . The spectroscopic signatures of I, Pb, N, and C are detected, together with those of O, F, and Al, the latter being not characteristic of the perovskite layer. A quantitative estimate of the relative concentration of elemental species is obtained from the measured spectroscopic intensities, corrected by the elemental and orbital specific photoemission cross sections.^{15,16} We obtain a I:Pb intensity ratio of 2.9 ± 0.1 , in good agreement with the MAPbI_3 stoichiometry, and a N:Pb ratio of 1.3 ± 0.1 , indicative of the presence of extra nitrogen species in the perovskite matrix, as discussed below. The C:N ratio shows the largest sample-to-sample variability and is generally larger than expected due to the strong extra contribution from carbon contamination, accounting for more than 50% of the C 1s photoemission intensity. The Al-related intensity and part of the O intensity are due to photoemission from the Al_2O_3 scaffold, while the remaining O intensity is due to contaminants too, as testified by a O:Al intensity ratio of 1.9 ± 0.1 , i.e., larger than expected from the 3:2 oxide stoichiometry. The presence of F can be explained with its segregation from the fluorine-doped tin oxide layer (see the Experimental Details section) during the annealing procedures. Cl is not detected in our photoemission experiment; i.e., the Cl concentration at the sample surface is below its detection limit (which is approximately 1% atomic concentration¹⁷). We compared the spectra acquired at normal emission to a new set of spectra (see Figure S1 in the Supporting Information) acquired at grazing emission. The depth probed by XPS is about 6 nm (i.e., 3 times the photoelectrons' inelastic mean free path¹⁸) and 3 nm at normal and grazing emission, respectively. We measure similar signal intensities for the photoemission from Pb, I, and N, indicative of a rather uniform perovskite composition with depth. Conversely, the O and C photoemission intensity is enhanced at grazing emission (especially for C), due to the contribution of surface species such as adsorbed water molecules, hydroxyl groups, or carbon-based molecules.

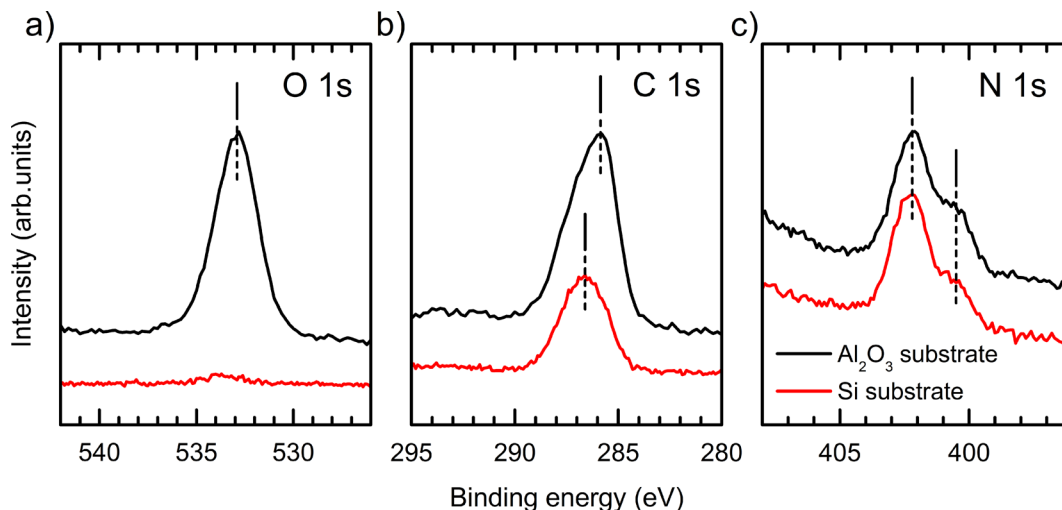


Figure 2. XPS O 1s (a), C 1s (b), and N 1s (c) profiles acquired from as-received $\text{CH}_3\text{NH}_3\text{PbI}_{3-x}\text{Cl}_x$ samples spin-coated on a Al_2O_3 scaffold (black lines) and vacuum evaporated on a flat Si substrate (red lines). The two set of spectra, vertically offset for clarity, have been normalized to the N 1s intensity.

The Pb 4f and I 3d spectra (see Figures S1a and S1b in the Supporting Information) are characterized by a spin-orbit split doublet, with the Pb 4f_{7/2} and I 3d_{5/2} peaks at a binding energy (BE) of 138.9 and 619.7 eV, respectively. These BE are consistent with literature estimates for bulk PbI_2 (see, e.g., ref 19 and references therein) and indicate the presence of I^- and Pb^{2+} species. According to the line shape analysis presented in the Supporting Information, the presence of chemically altered I and Pb species in the as-received samples is unlikely or close to the detection limit of our technique. In order to clarify the origin of the O and C signals, we compared the photoemission spectra from $\text{MAPbI}_{3-x}\text{Cl}_x$ perovskites spin-coated on meso-porous Al_2O_3 and those measured on perovskite samples evaporated on flat Si substrates. Vacuum evaporation guarantees a good thickness uniformity without the need of any oxide scaffold. The spectra acquired on Al_2O_3 - and Si-supported perovskites (black and red lines in Figure 2, respectively) are normalized to the N 1s intensity.

The O 1s spectrum (Figure 2a) from spin-coated samples shows a single peak at a BE of 532.9 eV, in analogy with the results of a recent XPS study describing the growth of Al_2O_3 on MAPbI_3 perovskites.²⁰ The O intensity is almost completely quenched on the evaporated samples, due to the removal of the alumina scaffold and to a negligible concentration of surface species. The C 1s spectrum (Figure 2b) is characterized by an asymmetric line shape peaking at 285.8 eV on Al_2O_3 -supported perovskites, while a symmetric peak centered at a BE of 286.6 eV is observed on the films evaporated on Si. According to the analysis of the O 1s line shape, the evaporated samples show an overall low concentration of surface contaminants. We therefore assign the C 1s peak at 286.6 eV mainly to photoemission from the perovskite molecules, while the feature at 285.8 eV observed for the spin-coated samples is likely to be related to C-based contaminants residing at the Al_2O_3 /perovskite or, for those portions of the Al_2O_3 scaffold left uncovered by the perovskite layer, Al_2O_3 /air interface. Our analysis is further supported by comparing the C 1s line shape at normal and grazing emission. The grazing-to-normal difference spectrum (shown in Figure S1d, after a proper intensity normalization) is proportional to the photoemission signal from surface species. Its shape, i.e., the presence of side

peaks and their relative intensity with respect to the main peak, located at a BE of 285.8 eV, is in good overall agreement with the C 1s spectra related to adventitious carbon usually reported for oxide surfaces.²¹ The C 1s BE is only slightly larger than the value of 285 eV conventionally assigned to carbon contamination,²² likely due to charging effects related to the insulating nature of Al_2O_3 .²³

The N 1s spectra from Al_2O_3 - and Si-supported perovskites (Figure 2c) are remarkably similar, and two features at BE of 402.2 and 400.5 eV are detected. A good agreement with the available literature data is obtained if the former feature (showing the largest photoemission intensity) is considered, yielding a C-to-N BE difference of 115.6 eV, close to the values of 115.7 and 115.9 eV from refs 24 and 25, related to either MAI molecules or MAPbI_3 perovskites. In addition, a N:Pb intensity ratio of 0.9 ± 0.1 is found by considering only the N signal from MAI molecules, in much better agreement with the expected MAPbI_3 stoichiometry with respect to our initial estimate. According to well-established models,^{26,27} the presence of the N 1s side peak at 400.5 eV in Figure 2c (with an intensity of about 30% of the whole N 1s peak intensity) is related to charge transfer to the N atom as a result of bond formation or breaking. In particular, a 1.5–2 eV BE shift (as in our case) for the N 1s peak is attributed to deprotonation of the methylammonium amino group.²⁸ According to ref 29, photoemission from methylamine molecules is characterized by a N-to-C BE difference of 114.1 eV, i.e., very close to the value of 113.9 eV we observe on the evaporated samples. We can therefore attribute the side N 1s peak to the presence of deprotonated ions, i.e. methylamine molecules, probably trapped within the perovskite crystal lattice. According to recent studies on the formation of the perovskite phase, excess molecular species might be produced from the decomposition of the precursor species following the reaction³⁰



The $\text{CH}_3\text{NH}_3\text{Cl}$ molecules can either (i) sublime during the annealing process or (ii) degrade into gaseous hydrochloric acid (HCl) and methylamine species.⁹ Our experimental results, i.e., the absence of Cl and the detection of a side

peak in the N 1s spectrum related to methylamine molecules, strongly indicate the dissociation of $\text{CH}_3\text{NH}_3\text{Cl}$ species. HCl molecules are comparatively smaller and more volatile and therefore are not detected within the depth probed in our experiment. The same issue has been recently investigated by means of thermogravimetric analysis. The authors of ref 31 detect a mass loss signal in $\text{MAPbI}_{3-x}\text{Cl}_x$ powders starting from about 250 °C. Such a temperature is well above the one characteristic of the annealing step involved in the perovskite preparation procedure, but it is below the threshold temperature for MAPbI_3 powders degradation. According to ref 31, the observed signal is likely related to the release of $\text{CH}_3\text{NH}_3\text{Cl}$ molecules from the perovskite bulk. Although the retrieved sublimation temperatures are higher with respect to those characteristic of thin films, due to the much lower surface-to-volume ratio,³⁰ this result fully supports our conclusion about the presence of excess molecular species within the perovskite matrix in the as-received samples. Such extra species might act as defect sites and therefore play an important role in defining the electronic behavior of such compounds. Organic–inorganic perovskites, for instance, show ambipolar characteristics (from p-type to intrinsic and n-type) depending on the growth conditions and, consequently, on the type and concentration of defect species in the bulk.³²

Effects of Surface Treatments on the Chemical and Electronic Properties of the Perovskite Surface. Figure 3 shows some XPS spectra related to a representative spin-coated sample as-received (black lines), submitted to *in situ* annealing (red lines) and, subsequently, to sputtering (green lines, see the Experimental Details section). Figure 3a shows the N 1s line shape together with the Pb 4d_{5/2} peak at about 414 eV. Their intensity ratio is representative of the compositional balance between the metal halide and the organic components of the hybrid perovskite layer. By comparing the relative intensities of the photoemission signal from N and Pb, it can be concluded that the annealing treatment dramatically reduces the concentration of MA ions, released from the perovskite in the form of methylamine and hydrogen iodide molecules.¹⁰ We note that even at the highest temperature explored, the overall C 1s intensity (not shown) is not significantly reduced; i.e. the annealing procedure does not remove the surface contamination. A subsequent sputtering treatment was therefore performed: in this way, it is possible to reduce the concentration of organic molecules and C and O containing contaminants on the surface close to the detection limit of our technique. The Pb 4d_{5/2} and Pb 4f spectra (Figures 3a and 3b, respectively) retain their original line shape after the annealing treatment, while the sputtering treatment promotes in both cases the formation of side peaks. Those additional signals have been highlighted in Figure 3 by numerically fitting the Pb 4d_{5/2} and Pb 4f spectra with two line shapes with similar spectral line width and, in the Pb 4f case, spin–orbit splitting according to the methodology described in the Supporting Information. The additional Pb 4f features, with 1.8 eV lower BE than the main doublet, indicate the presence of “metallic” Pb⁰ species.³³ The intensity of the photoemission signal pertaining to oxidized Pb²⁺ species is retrieved by integrating over the doublet at the highest BE. Starting from the stoichiometric perovskite surface, the above treatments lower the I:Pb²⁺ ratio from 2.9 ± 0.1 to 2.1 ± 0.1 for both the annealed and sputtered surfaces. The latter value is close to the 2:1 stoichiometry expected for PbI_2 . Another set of samples (results not shown) was submitted to a sputtering treatment without any previous annealing step: the

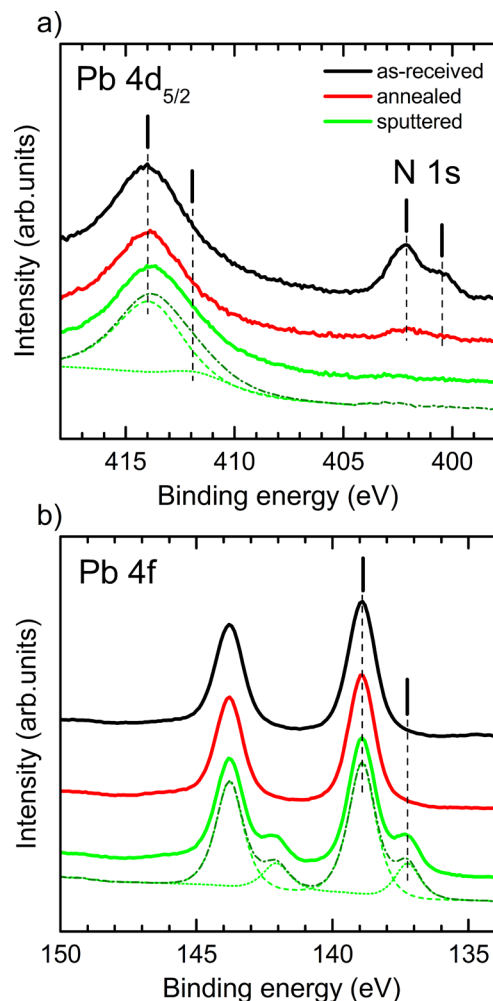


Figure 3. XPS N 1s (a) and Pb 4f (b) profiles acquired from a spin-coated $\text{CH}_3\text{NH}_3\text{PbI}_{3-x}\text{Cl}_x$ sample as-inserted (black), annealed for 1 h at 150 °C (red), and sputtered after the annealing (green), together with the line shape analysis performed on the spectra for the sputtered surface. Light green dashed lines: Pb^{2+} component; light green dotted lines: Pb^0 component; dark green lines: envelope functions. All spectra are normalized to the intensity of the Pb^{2+} component and have been vertically offset for clarity.

resulting XPS spectra are close to those shown in Figure 3 (green lines). The preferential sputtering³⁴ of C and N atoms upon Ar^+ bombardment of the perovskite surface is therefore observed, leading to the elimination of MA ions and eventually causing the collapse of the perovskite crystal lattice. By combining high temperature annealing and sputtering, it is therefore possible to efficiently promote the elimination of the MA species and to create a layer with the PbI_2 stoichiometry. Figure 4 compares the UPS spectra measured with He I photons on as-received (black), *in situ* annealed (red), and subsequently sputtered (green) perovskites. The valence electronic structure of organic perovskites is characterized by electron states related to the MA cations (located at BE higher than 6 eV) and by Pb and I derived states at a BE ranging from the valence band maximum (VBM) to 6 eV.^{37,38} A nil density of states is observed in our experiments from the VBM up to the position of the sample Fermi energy (E_F) for as-received perovskites. Peak *a* is associated with photoemission from C valence orbitals, while peak *b* is more likely related to N valence orbitals.³⁸ The position of the VBM is at 1.7 eV below E_F (see

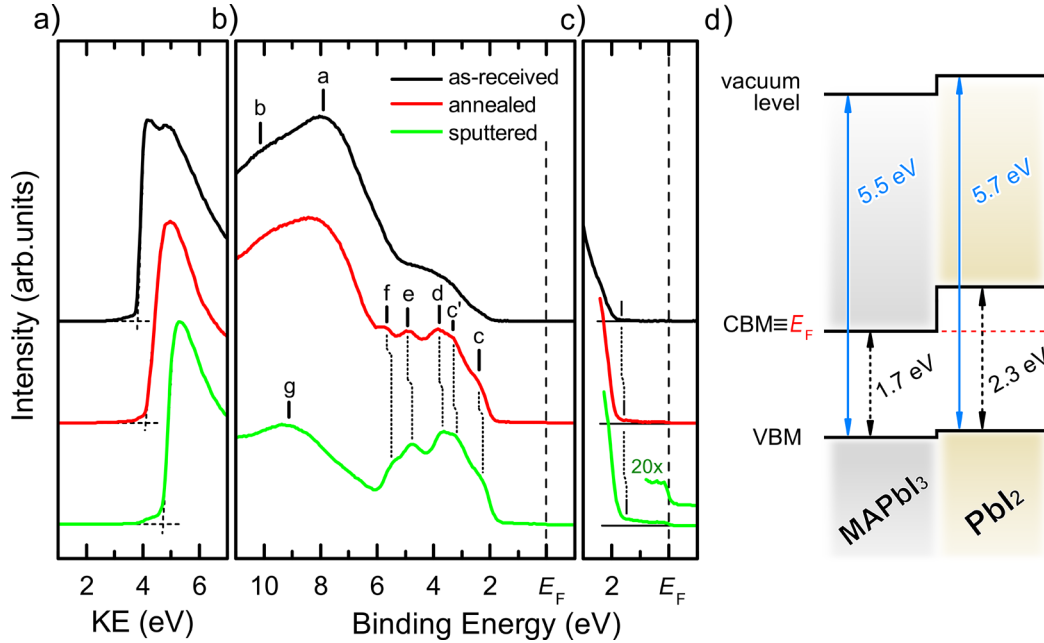


Figure 4. (a) Intensity of secondary electron emission upon He I excitation, as a function of the kinetic energy of the photoelectrons, measured with respect to the sample E_F . The photoemission onset gives directly the work function (Φ). (b) UPS valence band (He I photons) of a spin-coated $\text{CH}_3\text{NH}_3\text{PbI}_{3-x}\text{Cl}_x$ sample as-received (black), annealed for 1 h at 150 °C (red) and sputtered (green). Letters from *a* to *g* mark the position of relevant features: (*a*, *b*) photoemission from C and N related orbitals; (*c*, *c'*) photoemission from the hybrid Pb 6s–I 5sp₃ antibonding orbital; (*d*–*f*) photoemission from I 5p orbitals, and (*g*) photoemission from the bonding Pb 6s–I 5sp₃ orbitals.^{35,36} (c) Magnified portion of the BE region close to E_F showing the position of the valence band maximum (VBM). (d) Schematic diagram showing the alignment of the relevant electronic states at the $\text{MAPbI}_3/\text{PbI}_2$ interface (CBM = conduction band minimum).

Figure S3 in the Supporting Information for more details). The conduction band minimum (CBM), obtained by adding the electronic band gap (about 1.7 eV from ref 39) to the VBM,⁴⁰ is therefore coincident with E_F . Our results are compatible with the strong n-type behavior already observed for Al_2O_3 supported MAPbI_3 ⁴¹ and $\text{MAPbI}_{3-x}\text{Cl}_x$ ⁴² perovskites, possibly due to a high concentration of donor-like states related to defects.^{33,42} We recall that negligible differences (within the accuracy of our characterization) are observed in the literature between the electronic structure of MAPbI_3 and $\text{MAPbI}_{3-x}\text{Cl}_x$ perovskite surfaces.³⁹ In the following, we will therefore refer to the topmost perovskite layers as to the MAPbI_3 surface. *In situ* treatments progressively increase the contribution of Pb and I derived states to the valence electronic structure and enhance fine details in the BE range below 6 eV. A series of small additional features are observed after annealing for 1 h at 150 °C (letters from *c* to *f* in Figure 4); however, the line shape observed in Figure 4b for the annealed sample is still dominated by photoemission from organic species. After the sputtering treatment, the BE of the observed features (Figure 4b, green line) and the overall photoemission line shape indicate the formation of a PbI_2 layer^{35,36} (see Figure 4 for more details). The VBM is only slightly affected by the surface modifications and is seen to shift (Figure 4c) by about 0.1(0.2) eV toward lower BE on the annealed (sputtered) sample. Furthermore, in the sputtered sample a faint intensity tail is seen to extend from the VBM toward E_F , where a metallic edge is observed, consistent with the observation of reduced Pb species in Figure 3. The photoemission signal from secondary electrons (Figure 4a) is used to obtain the work function (Φ) of the perovskite samples. Considering the VBM position determined for the spectra of Figure 4c, an ionization potential (IP = Φ + VBM) of 5.5 eV is estimated for the as-received samples, in good

agreement with other photoemission-based results for either Al_2O_3 or TiO_2 supported organic perovskites.^{39,41,43} The IP of the annealed and sputtered sample increases to 5.7 and 6.2 eV, respectively, consistent with the larger IP reported in the literature for PbI_2 .^{10,36} Starting from the experimental determination of the VBM and Φ values for the as-received and annealed samples (i.e., the MAPbI_3 and PbI_2 surfaces, respectively), the schematic diagram of Figure 4d has been obtained. The CBM for the annealed surface is about 0.7 eV above E_F , accounting for the PbI_2 bandgap (2.3 eV, from optical measurements⁴⁴). A type II (or “staggered”) band alignment at the $\text{MAPbI}_3/\text{PbI}_2$ interface is therefore realized. We note some discrepancies with a previous study on the same interface,¹⁰ where type I band alignment was predicted on the basis of the simplifying assumption of vacuum levels equalization between MAPbI_3 and PbI_2 . The use of an experimentally determined common reference energy (E_F) and the *in situ* processing of the perovskite surface allows us to detect a significant energy imbalance in the vacuum levels,⁴⁵ which results in a net upward shift of the PbI_2 bands. This proves that no barrier is actually present for hole injection into the PbI_2 layer, at variance with the conclusions of ref 10. In photovoltaic devices, the perovskite layers are further processed by spin-coating on top (i.e., on the MAPbI_3 surface) an organic hole transport material (HTM). Consider for instance 2,2',7,7'-tetrakis(*N,N*-di-*p*-methoxyphenylamine)-9,9'-spirobifluorene, or spiro-MeOTAD, characterized by a highest occupied molecular orbital (HOMO) BE of about 1 eV.³⁹ According to the schematic diagram of Figure 4d, the thin PbI_2 layer acts toward promoting hole injection into the HTM and reducing charge recombination by retaining electrons in the perovskite layer.

CONCLUSIONS

We have analyzed the chemical and electronic properties of MAPbI_{3-x}Cl_x perovskite films either spin-coated on mesoporous alumina or evaporated on Si substrates. Our findings strongly contribute to the current understanding of both the physicochemical behavior of organic-inorganic perovskites and the operation of the related photovoltaic devices. In particular, (i) we detect the presence of neutral methylamine molecules and explain their formation and the elimination of Cl species from the perovskite layer with the decomposition of methylammonium chloride during the film preparation. It is likely that such molecules play a role in determining the complex defect mechanisms at the basis of the electronic behavior of MAPbI_{3-x}Cl_x perovskites. Furthermore, (ii) we characterized the thin PbI₂ layer formed at the perovskite surface upon *in situ* annealing and sputtering, considering in particular the band alignment at the MAPbI₃/PbI₂ interface. According to our results, the PbI₂ layer can be implemented in devices as an electron blocking/hole injecting layer for the efficient collection of photogenerated holes from MAPbI₃ perovskites.

ASSOCIATED CONTENT

The detailed line shape analysis of the XPS spectra from a representative as-received perovskite sample is included (PDF).

AUTHOR INFORMATION

Corresponding Author

*E-mail alberto.calloni@polimi.it; Ph +39.02.2399.6566; Fax +39.02.2399.6129 (A.C.).

Notes

The authors declare no competing financial interest.

ACKNOWLEDGMENTS

The research of A.C. is funded by Fondazione Cariplo (2013 SHAPES project). A.A. has received funding from the European Union's Seventh Framework Programme for research, technological development, and demonstration under grant agreement no. 291771.

REFERENCES

- (1) Park, N.-G. Perovskite Solar Cells: An Emerging Photovoltaic Technology. *Mater. Today* **2015**, *18*, 65–72.
- (2) National Center for Photovoltaics (U.S. Department of Energy), Research Cell Efficiency Records Chart (accessed July 16, 2015); http://www.nrel.gov/ncpv/images/efficiency_chart.jpg.
- (3) Lee, M. M.; Teuscher, J.; Miyasaka, T.; Murakami, T. N.; Snaith, H. J. Efficient Hybrid Solar Cells Based on Meso-Superstructured Organometal Halide Perovskites. *Science* **2012**, *338*, 643–647.
- (4) Burschka, J.; Pellet, N.; Moon, S.-J.; Humphry-Baker, R.; Gao, P.; Nazeeruddin, M. K.; Grätzel, M. Sequential Deposition as a Route to High-Performance Perovskite-Sensitized Solar Cells. *Nature* **2013**, *499*, 316–319.
- (5) Liu, M.; Johnston, M. B.; Snaith, H. J. Efficient Planar Heterojunction Perovskite Solar Cells by Vapour Deposition. *Nature* **2013**, *501*, 395–398.
- (6) Sutherland, B. R.; Hoogland, S.; Adachi, M. M.; Kanjanaboos, P.; Wong, C. T. O.; McDowell, J. J.; Xu, J.; Voznyy, O.; Ning, Z.; Houtepen, A. J.; et al. Perovskite Thin Films via Atomic Layer Deposition. *Adv. Mater.* **2015**, *27*, 53–58.
- (7) Chen, Q.; Zhou, H.; Hong, Z.; Luo, S.; Duan, H.-S.; Wang, H.-H.; Liu, Y.; Li, G.; Yang, Y. Planar Heterojunction Perovskite Solar Cells via Vapor-Assisted Solution Process. *J. Am. Chem. Soc.* **2014**, *136*, 622–625.
- (8) Stranks, S. D.; Eperon, G. E.; Grancini, G.; Menelaou, C.; Alcocer, M. J. P.; Leijtens, T.; Herz, L. M.; Petrozza, A.; Snaith, H. J. Electron-Hole Diffusion Lengths Exceeding 1 Micrometer in an Organometal Trihalide Perovskite Absorber. *Science* **2013**, *342*, 341–344.
- (9) Williams, S. T.; Zuo, F.; Chueh, C.-C.; Liao, C.-Y.; Liang, P.-W.; Jen, A. K.-Y. Role of Chloride in the Morphological Evolution of Organo-Lead Halide Perovskite Thin Films. *ACS Nano* **2014**, *8*, 10640–10654.
- (10) Chen, Q.; Zhou, H.; Song, T.-B.; Luo, S.; Hong, Z.; Duan, H.-S.; Dou, L.; Liu, Y.; Yang, Y. Controllable Self-Induced Passivation of Hybrid Lead Iodide Perovskites toward High Performance Solar Cells. *Nano Lett.* **2014**, *14*, 4158–4163.
- (11) Supasai, T.; Rujisamphan, N.; Ullrich, K.; Chemseddine, A.; Dittrich, T. Formation of a Passivating CH₃NH₃PbI₃/PbI₂ Interface during Moderate Heating of CH₃NH₃PbI₃ Layers. *Appl. Phys. Lett.* **2013**, *103*, 183906/1–183906/3.
- (12) Ball, J. M.; Lee, M. M.; Hey, A.; Snaith, H. J. Low-Temperature Processed Meso-Superstructured to Thin-Film Perovskite Solar Cells. *Energy Environ. Sci.* **2013**, *6*, 1739–1743.
- (13) Berti, G.; Calloni, A.; Brambilla, A.; Bussetti, G.; Duò, L.; Ciccacci, F. Direct Observation of Spin-Resolved Full and Empty Electron States in Ferromagnetic Surfaces. *Rev. Sci. Instrum.* **2014**, *85*, 073901/1–073901/4.
- (14) Helander, M. G.; Greiner, M. T.; Wang, Z. B.; Lu, Z. H. Pitfalls in Measuring Work Function Using Photoelectron Spectroscopy. *Appl. Surf. Sci.* **2010**, *256*, 2602–2605.
- (15) Yeh, J. J.; Lindau, I. Atomic Subshell Photoionization Cross Sections and Asymmetry Parameters: 1 ≤ Z ≤ 103. *At. Data Nucl. Data Tables* **1985**, *32*, 1–155.
- (16) Manson, S. T. Dependence of the Angular Distribution of Atomic Photoelectrons on Energy and Z. *J. Electron Spectrosc. Relat. Phenom.* **1972**, *1*, 413–438.
- (17) Shard, A. G. Detection Limits in XPS for More than 6000 Binary Systems Using Al and Mg K α X-Rays. *Surf. Interface Anal.* **2014**, *46*, 175–185.
- (18) Tanuma, S.; Powell, C. J.; Penn, D. R. Calculations of Electron Inelastic Mean Free Paths. V. Data for 14 Organic Compounds over the 50–2000 eV Range. *Surf. Interface Anal.* **1994**, *21*, 165–176.
- (19) Yang, C.-H.; Yau, S.-L.; Fan, L.-J.; Yang, Y.-W. Deposition of Lead Iodide Films on Rh(100) Electrodes from Colloidal Solutions—the Effect of an Iodine Adlayer. *Surf. Sci.* **2003**, *540*, 274–284.
- (20) Niu, G.; Li, W.; Meng, F.; Wang, L.; Dong, H.; Qiu, Y. Study on the Stability of CH₃NH₃PbI₃ Films and the Effect of Post-Modification by Aluminum Oxide in All-Solid-State Hybrid Solar Cells. *J. Mater. Chem. A* **2014**, *2*, 705–710.
- (21) McCafferty, E.; Wightman, J. P. Determination of the Concentration of Surface Hydroxyl Groups on Metal Oxide Films by a Quantitative XPS Method. *Surf. Interface Anal.* **1998**, *26*, 549–564.
- (22) Swift, P. Adventitious Carbon—the Panacea for Energy Referencing? *Surf. Interface Anal.* **1982**, *4*, 47–51.
- (23) We note that similar to the C 1s case, also Al₂O₃-related features in the O 1s and Al 2p spectral regions are similarly shifted toward larger BE with respect to the literature.
- (24) Ng, T.-W.; Chan, C.-Y.; Lo, M.-F.; Guan, Z. Q.; Lee, C. Formation Chemistry of Perovskites with Mixed Iodide/chloride Content and the Implications on Charge Transport Properties. *J. Mater. Chem. A* **2015**, *3*, 9081–9085.
- (25) Chen, S.; Goh, T. W.; Sabba, D.; Chua, J.; Mathews, N.; Huan, C. H. A.; Sum, T. C. Energy Level Alignment at the Methylammonium Lead Iodide/copper Phthalocyanine Interface. *APL Mater.* **2014**, *2*, 081512/1–081512/7.

- (26) Siegbahn, K.; Nordling, C.; Fahlman, A.; Nordberg, R.; Hamrin, K.; Hedman, J.; Johansson, G.; Bergma, T. *ESCA: Atomic, Molecular and Solid State Structure Studied by Means of Electron Spectroscopy*; Almqvist & Wiksells: Upsala, 1967.
- (27) Calloni, A.; Brambilla, A.; Berti, G.; Bussetti, G.; Canesi, E. V.; Binda, M.; Petrozza, A.; Finazzi, M.; Ciccacci, F.; Duò, L. X-Ray Photoemission Spectroscopy Investigation of the Interaction between 4-Mercaptopyridine and the Anatase TiO₂ Surface. *Langmuir* **2013**, *29*, 8302–8310.
- (28) Song, X.; Ma, Y.; Wang, C.; Dietrich, P. M.; Unger, W. E. S.; Luo, Y. Effects of Protonation, Hydrogen Bonding, and Photo-damaging on X-Ray Spectroscopy of the Amine Terminal Group in Aminothiolate Monolayers. *J. Phys. Chem. C* **2012**, *116*, 12649–12654.
- (29) Chen, J. J.; Winograd, N. The Adsorption and Decomposition of Methylamine on Pd{111}. *Surf. Sci.* **1995**, *326*, 285–300.
- (30) Yu, H.; Wang, F.; Xie, F.; Li, W.; Chen, J.; Zhao, N. The Role of Chlorine in the Formation Process of “CH₃NH₃PbI_{3-x}Cl_x” Perovskite. *Adv. Funct. Mater.* **2014**, *24*, 7102–7108.
- (31) Dualeh, A.; Gao, P.; Seok, S. Il; Nazeeruddin, M. K.; Grätzel, M. Thermal Behavior of Methylammonium Lead-Trihalide Perovskite Photovoltaic Light Harvesters. *Chem. Mater.* **2014**, *26*, 6160–6164.
- (32) Yin, W.-J.; Shi, T.; Yan, Y. Unusual Defect Physics in CH₃NH₃PbI₃ Perovskite Solar Cell Absorber. *Appl. Phys. Lett.* **2014**, *104*, 063903/1–063903/4.
- (33) Conings, B.; Baeten, L.; De Dobbelaere, C.; D’Haen, J.; Manca, J.; Boyen, H.-G. Perovskite-Based Hybrid Solar Cells Exceeding 10% Efficiency with High Reproducibility Using a Thin Film Sandwich Approach. *Adv. Mater.* **2014**, *26*, 2041–2046.
- (34) Brambilla, A.; Calloni, A.; Aluicio-Sardui, E.; Berti, G.; Kan, Z.; Beaupré, S.; Leclerc, M.; Butt, H.-J.; Floudas, G.; Keivanidis, P. E.; et al. X-Ray Photoemission Spectroscopy Study of Vertical Phase Separation in F8BT:PDI/ITO Films for Photovoltaic Applications. In *SPIE NanoScience + Engineering*; Banerji, N., Hayes, S. C., Silva, C., Eds.; International Society for Optics and Photonics: Bellingham, WA, 2014; pp 91650C/1–91650C/9.
- (35) Margaritondo, G.; Rowe, J.; Schlüter, M.; Wertheim, G.; Levy, F.; Mooser, E. Photoemission Spectroscopy of Layered Halides: PbI₂ and BiI₃. *Phys. Rev. B* **1977**, *16*, 2934–2937.
- (36) Margaritondo, G.; Rowe, J. Synchrotron-Radiation Photoemission Spectroscopy of Octahedrally Coordinated Layer Compounds. *Phys. Rev. B: Condens. Matter Mater. Phys.* **1979**, *19*, 3266–3275.
- (37) Mosconi, E.; Amat, A.; Nazeeruddin, M. K.; Grätzel, M.; De Angelis, F. First-Principles Modeling of Mixed Halide Organometal Perovskites for Photovoltaic Applications. *J. Phys. Chem. C* **2013**, *117*, 13902–13913.
- (38) Lindblad, R.; Bi, D.; Park, B.; Oscarsson, J.; Gorgoi, M.; Siegbahn, H.; Odelius, M.; Johansson, E. M. J.; Rensmo, H. Electronic Structure of TiO₂/CH₃NH₃PbI₃ Perovskite Solar Cell Interfaces. *J. Phys. Chem. Lett.* **2014**, *5*, 648–653.
- (39) Schulz, P.; Edri, E.; Kirmayer, S.; Hodes, G.; Cahen, D.; Kahn, A. Interface Energetics in Organo-Metal Halide Perovskite-Based Photovoltaic Cells. *Energy Environ. Sci.* **2014**, *7*, 1377–1381.
- (40) The perovskite bandgap measured with photoemission is related to single-particle excitations and is therefore intrinsically larger than the reported optical bandgap (about 1.55 eV from ref 3), which accounts for the formation of a bound electron–hole pair upon optical excitation.
- (41) Miller, E.; Zhao, Y.; Mercado, C.; Saha, S.; Luther, J. M.; Zhu, K.; Stevanovic, V.; Perkins, C. L.; van de Lagemaat, J. Substrate-Controlled Band Positions in CH₃NH₃PbI₃ Perovskite Films. *Phys. Chem. Chem. Phys.* **2014**, *16*, 22122–22130.
- (42) Leijtens, T.; Stranks, S. D.; Eperon, G. E.; Lindblad, R.; Johansson, E. M. J.; McPherson, I. J.; Rensmo, H.; Ball, J. M.; Lee, M. M.; Snaith, H. J. Electronic Properties of Meso-Superstructured and Planar Organometal Halide Perovskite Films: Charge Trapping, Photodoping, and Carrier Mobility. *ACS Nano* **2014**, *8*, 7147–7155.
- (43) Kim, H.-S.; Lee, C.-R.; Im, J.-H.; Lee, K.-B.; Moehl, T.; Marchioro, A.; Moon, S.-J.; Humphry-Baker, R.; Yum, J.-H.; Moser, J. E.; et al. Lead Iodide Perovskite Sensitized All-Solid-State Submicron Thin Film Mesoscopic Solar Cell with Efficiency Exceeding 9%. *Sci. Rep.* **2012**, *2*, 591/1–591/7.
- (44) Ferreira da Silva, A.; Veissid, N.; An, C. Y.; Pepe, I.; Barros de Oliveira, N.; Batista da Silva, A. V. Optical Determination of the Direct Bandgap Energy of Lead Iodide Crystals. *Appl. Phys. Lett.* **1996**, *69*, 1930–1932.
- (45) Calloni, A.; Berti, G.; Ferrari, A.; Brambilla, A.; Bussetti, G.; Canesi, E. V.; Petrozza, A.; Duò, L. Photoemission Study of the Poly(3-hexylthiophene)/TiO₂ Interface and the Role of 4-Mercaptopyridine. *Thin Solid Films* **2014**, *560*, 39–43.